Probing dynamics in the Franck–Condon and exit channel regions of dissociating H_2S: Emission spectra upon tunable excitation from 199–203 nm

P. W. Browning, E. Jensen, G. C. G. Waschewsky, M. R. Tate, and L. J. Butler
The James Franck Institute and Department of Chemistry, The University of Chicago, Chicago, Illinois 60637

J. P. Hessler
Chemistry Division, Argonne National Laboratory, Argonne, Illinois 60439

(Received 18 May 1994; accepted 15 June 1994)

This study uses emission spectroscopy of H_2S at excitation energies near 200 nm to probe the dissociation dynamics from a conical intersection in the Franck–Condon region to the H+SH product exit channel. Photoexcitation accesses these coupled surfaces near the transition state region of the lower adiabat, a potential surface for the excited state H+SH→HS+H reaction. Excitation wavelengths from 199–203 nm tune through the first of the resonances in the absorption spectrum assigned to recurrences in the motion along the symmetric stretch orthogonal to the reaction coordinate and also access energies just above and at the conical intersection. We disperse the emission from the dissociating molecules at each of five excitation wavelengths in this region to probe several features of the reaction dynamics on the coupled potential energy surfaces. The resulting emission spectra cover the range of final vibrational eigenstates from 500 to 11 000 cm^{-1} above the initial ground vibrational state for all five excitation wavelengths, and go out to 16 500 cm^{-1} for the 199 and 201 nm excitation wavelengths. The resulting spectra, when considered in conjunction with recent scattering calculations by Heumann and Schinke on *ab initio* potential energy surfaces for this system, evidence a progression of emission features to low vibrational eigenstates in the SH stretch that result from coupling of the nuclear motion from the bound to the dissociative region of the potential energy surfaces. This emission, into local mode eigenstates such as 00^+1, 11^+0, 11^+1, 21^+0, 21^+1, evidences the antisymmetric dissociative motion and bending induced near the conical intersection, and dominates the spectrum at excitation wavelengths only near 200 nm. We analyze the excitation wavelength dependence of these features and also of the $n0^+0$ progression for $n \geqslant 4$, which reflect the exit channel dynamics. The excitation wavelength dependence shows that while the emission spectra do not reveal any dynamics unique to scattering states that access a symmetric stretch resonance in the Franck–Condon region, they do reveal the energy location of and the dynamics at the conical intersection. A reanalysis of other workers' measurements of the SH product vibrational state distribution shows that $v=0$ products are strongly favored at excitation wavelengths near the conical intersection.

I. INTRODUCTION

In triatomic reactive scattering systems such as $F+H_2$ and $H+H_2$, the comparison between experiments that probe various regions of the reactive potential energy surface and predictions from exact reactive scattering calculations on *ab initio* potential energy surfaces has met with considerable success.[1,2] While early studies of triatomic reactive scattering often assumed that the dynamics could be modeled on a single Born–Oppenheimer potential energy surface, experiments and theory have begun to reveal the importance of electronically nonadiabatic effects for many chemical reactions.[3–5] The photoexcitation of H_2S in its first absorption band[6,7] allows us to access, near the Franck–Condon region, the saddle point of the excited state H+SH reaction coordinate,[8,9] and the resulting emission spectra allow us to probe regions of the reactive scattering wave functions sensitive to nonadiabatic coupling between two potential energy surfaces near the transition state region and to the dynamics in the H+SH exit channel. The data is of particular interest in comparison with the absorption and emission spectra and photodissociation dynamics of H_2O, which have been successfully modeled by including only one Born–Oppenheimer potential energy surface.[10] While the first ultraviolet absorption bands are similar for these two systems,[6,7,10] evidencing weak resonances due to recurrence in the symmetric stretch motion near the saddle point on the excited electronic potential energy surfaces,[9,11–14] the emission spectra[11,12,15] differ dramatically. In analyzing these differences, it is important to consider the electronic character of the bound and dissociative potential energy surfaces accessed in H_2S as compared to H_2O, and how that electronic character changes from the Franck–Condon region to the exit channel. We attempt in this paper to present a coherent model to understand the previous data available on these systems and we provide new H_2S emission spectroscopy data sensitive to the nonadiabatic dynamics on the conically intersecting potential energy surfaces near the transition state for the H+SH→HS+H excited state reaction coordinate.

While the excited electronic state accessed in the photodissociation of H_2O in its first absorption band is a mixed

 0021-9606/94/101(7)/5652/13/$6.00

Rydberg/valence state with $^1B_1$ symmetry in C_{2v}, recent *ab initio* calculations[16–18] have demonstrated that electronic configurations of both $^1B_1$ and $^1A_2$ symmetry are important in the photodissociation of H_2S (the $^1A_2$ excited electronic state is much higher in energy in the Franck–Condon region in H_2O). There have been a few different models proposed to understand the experimental absorption and emission spectra[7,9,11,15] and photofragment rovibrational state distribution data[19–23] available for H_2S excited in this band. Schinke and co-workers[16–18] have calculated potential energy surfaces in three dimensions for the ground and first two excited states of H_2S. They transform calculated adiabats, transition dipole moments and coupling matrix elements for the two potential energy surfaces to an approximately diabatic representation in order to use a time-dependent quantum scattering method, including all three internuclear degrees of freedom, to calculate an absorption profile as well as product distributions resulting from photodissociation on these coupled surfaces. These calculations have resulted in a much better understanding of the photodissociation of H_2S, but the difficulty of calculating and interpreting dynamical processes involving such closely spaced and strongly coupled states has led to some persistent conjecture. Schinke and co-workers produce *ab initio* surfaces which support earlier models[19,24] describing the photodissociation of H_2S as an allowed photoabsorption to a bright bound state of $^1B_1$ symmetry, strongly predissociated by a dissociative dark state of $^1A_2$ symmetry. Dixon and co-workers,[25] however, propose an alternative model developed using time dependent quantum mechanical calculations on adjustable potential energy surfaces. This model, in contrast to most other descriptions, interprets the photodissociation of H_2S as excitation to a bright dissociative state of $^1B_1$ symmetry which is perturbed due to a Fano bound-continuum mechanism,[26] by weak coupling to a quasibound state of $^1A_2$ symmetry. This proposed excitation to a predominantly dissociative $^1B_1$ state is reminiscent of the photodissociation of H_2O. But in order to maintain the diffuseness of the absorption spectrum and simultaneously accommodate this scenario involving weak coupling to another state, they must invoke some mechanism for flux loss from the dark state. Dixon *et al.* propose either dissociation along a different channel: $H_2S \rightarrow H_2 + S$, (energetically allowed, but not yet observed experimentally) or recrossing to the $^1B_1$ state outside of the Franck–Condon region.

The emission spectroscopy[27] measurements presented in this paper, analyzed in comparison with more recent time-dependent dynamics calculations[18] by Heumann and Schinke and in conjunction with some simple *ab initio* electronic structure calculations done here, are designed to investigate the short time dissociation dynamics of H_2S on the conically intersecting potential energy surfaces. Earlier measurements of the emission spectra involved excitation of H_2S only at certain energies in the absorption band achievable with an ArF excimer laser or at the discrete energies obtained by Raman shifting the fourth harmonic of a Nd:YAG laser. The present emission spectroscopy experiments, using excitation wavelengths tunable between 199 and 203 nm, allowed us to address some of the unresolved questions from the earlier theoretical and experimental work. The first emission spectrum of dissociating H_2S,[11] using the ArF excitation wavelength of 193.3 nm, evidenced two features of the dissociation dynamics. The early portion of the emission spectrum showed emission to a progression of H_2S stretching motion assigned to increasing quanta in the symmetric stretch normal mode as well as some emission to states assigned in a normal mode representation as combinations of the symmetric stretch and the antisymmetric stretch with one quantum of bend. The early features in this spectrum demonstrate that the recurrences in the absorption spectrum, which had been falsely attributed to recurrences along the bending coordinate, are more likely due to recurrences along the symmetric stretch coordinate. (While the emission spectrum shows some activity in the bending mode, there is no long progression along this coordinate as might be expected if motion along this coordinate were truly responsible for the recurrences.) At larger Raman shifts, roughly corresponding to later times in the photodissociation event, the emission into a progression of increasing quanta of S–H stretching vibrational eigenstates[28,29] is clarified by reassignment in the local mode representation. (The zeroth-order description of these eigenstates as local mode states nm^+b, where n and m are the quanta in each S–H local oscillator and b is quanta of bending motion, becomes more accurate with increasing quanta of vibration.[29]). The dominant features in this part of the spectrum were interpreted as evidencing exit channel dynamics. Preferential emission into vibrational eigenstates with increasing quanta in only one S–H oscillator and no quanta in the bend ($n0^+0$ with $n=6$ and 7) showed that the dynamics has evolved from symmetric stretching in the Franck–Condon region to dynamics in the exit channel where there is little motion in the S–H bond which becomes the SH diatomic fragment and no bending motion, consistent with the low vibrational and rotational excitation observed in final product studies.[19–23] Shortly following these studies, Brudzynski *et al.* obtained the emission spectra of H_2S at nine other wavelengths stretching across the whole absorption profile.[15] They noticed a large variation in the intensities of the emission features as they changed the wavelength of excitation. The spectra are dominated by stretching modes, yet also show some activity in combination bands involving one quantum of bend and multiple quanta of stretch. The spectrum furthest to the red at 223 nm shows emission into the 10^+0, 20^+0, and 30^+0 bands and little else. As they tune to shorter wavelengths, Brudzynski *et al.* start to see emission intensity into the 11^+0, 10^+1, and 21^+0 bands as well as other nm^+b combinations with zero or one quantum of bend as their spectra extend to greater Raman shifts. They also see a large increase in the bending fundamental, 00^+1, as well as the first bend and stretch combination band, 10^+1, growing up to and peaking near 204 to 200 nm. As they move out to 184 nm, the spectrum is again dominated by $n0^+0$ features. They interpret their spectra on the basis of two overlapping states, a dissociative B_1 state "directly analogous to the $\tilde{A}$ state of water and, at slightly higher in energy at the vertical geometry, a state of A_2 symmetry giving rise to a forbidden transition to a bound or quasibound surface." Thus, their model is again different from the one proposed in the para-

graphs above. They do not comment on a feature of their emission spectra that the present studies show is very important. The emission spectra upon excitation at 200 nm look qualitatively different from all the others; it is the only one in which the 11^+0 emission band is larger than the 20^+0 feature and the 21^+0 band is larger than the 30^+0 feature. In order to assess whether these and other differences are due to an accidental coincidence of the 200 nm excitation wavelength (one of the Raman shifted wavelengths of the Nd:YAG fourth harmonic) with the $v=0$ resonance in the symmetric stretch in the absorption spectrum, or whether they result from a different feature of the dynamics on the conically intersecting surfaces, it is essential to be able to tune the excitation wavelength through a resonance in the absorption spectrum.

The experiment presented here uses tunable ultraviolet excitation between 199 and 203 nm to access the coupled excited potential energy surfaces at several energies, allowing us to tune through excitation energies below, on resonance with, and above the first of the symmetric stretch resonances in the absorption spectrum. At each excitation energy, we disperse the emission from the dissociating molecules to probe the evolution of the dynamics from the Franck–Condon region into the exit channel of the reactive trajectories. We wished to address three questions with these measurements: (1) Can the data discern any exit channel dynamics unique to scattering states that access a symmetric stretch resonance in the Franck–Condon region? (This is a complement of the usual question posed—do state selected reactants or products map to particular scattering resonances in the transition state region?) (2) Can we probe the influence of the conical intersection via emission spectroscopy? (3) Can we elucidate how the dynamics changes from outward motion in the symmetric stretch in the Franck–Condon region to exit channel dynamics that give vibrationally and rotationally cold SH fragments? The resulting spectra, when considered in conjunction with more recent scattering calculations,[18] clearly evidence emission features characteristic of nonadiabatic dynamics near the conical intersection between the $^1B_1$ and $^1A_2$ surfaces. We also present some simple *ab initio* calculations of the dominant electronic configurations contributing to the bound and dissociative adiabatic potential energy surfaces in the Franck–Condon and exit channel regions that give valuable insight for interpretation of the spectra.

II. EXPERIMENTAL METHOD

To excite H_2S at various wavelengths near 200 nm in the first absorption band, we triple the output of a Lambda Physik FL3002 dye laser to generate tunable light between 199 and 203 nm. This dye laser is pumped with the frequency doubled output of a Quantel YG 581-C Nd:YAG laser operating at 20 Hz, giving pulses of about 20 ns at 350 mJ/pulse. Rhodamine 610 is used with an intracavity etalon to produce 600 nm light with a pulse-averaged bandwidth of about 0.05 cm^{-1}. Two stages of amplification increase the energy to approximately 40 mJ/pulse. The light is tripled in two steps.[30] A potassium–dihydrogen phosphate crystal is used to generate 3.5 mJ/pulse ultraviolet light near 300 nm. A dichroic beam splitter then separates the ultraviolet and residual visible beams, thereby allowing us to rotate the polarization of the visible beam with a half-wave plate. The two beams are then recombined with a second dichroic mirror and colinearly sent into a beta–barium borate (BBO) crystal which generates the light between 199 and 203 nm with energies up to 150 μJ/pulse. The range of excitation is limited on the short wavelength side by the onset of absorption by the BBO crystal and beyond 203 nm by the precipitous decrease in the absorption cross section of H_2S. With these conditions we were able to obtain emission spectra with Raman shifts up to 11 000 cm^{-1}. To obtain emission spectra with larger Raman shifts when exciting at 199 and 201 nm we increased the output from the dye laser to 60 mJ/pulse to produce up to 250 μJ/pulse of third harmonic light.

The tunable 200 nm light excites room temperature gaseous H_2S in a flow cell, and the resulting emission is collected at 90° to the direction of propagation of the excitation beam and detected with an EG&G 1455B-700-HQ optical multichannel analyzer (OMA). First, the tunable light near 200 nm is separated from the residual visible and ultraviolet light by dispersion in a Pellin–Broca (constant deviation) prism and then directed into a stainless steel cell where it photoexcites flowing H_2S gas. We flow 300 mtorr of H_2S obtained from Matheson at 95% purity, and flush the sidearms with 6 torr of helium. Emitted light is recollimated, passed through a depolarizing wedge, and focused onto the 75 μm entrance slit of a Spectra-Pro 0.275 m spectrometer. A Milton–Roy 1200 groove/mm holographic grating disperses the emission in first order onto the 18 mm microchannel plate image intensifier of the OMA. The detector collects a 50 nm wide spectrum for each exposure with a resolution of 75 cm^{-1} near 200 nm. For each exposure of 300 s (6000 laser shots), we gate the image intensifier of the OMA with a gate synched to the laser. We then sum approximately 100 exposures to obtain a spectrum averaged over 600 000 shots for each excitation wavelength.

III. COMPUTATIONAL METHOD

To help interpret the experimental results, we also present *ab initio* electronic structure calculations for the excited electronic states of H_2O and H_2S using the Gaussian 92 system of programs.[31] The aim is not to improve on the already highly accurate excited state potential energy surfaces, but rather to get a feel for the change in character of the dominant electronic configurations characterizing the bound and repulsive adiabatic potential energy surfaces in the Franck–Condon region and in the H+SH exit channel. The configuration interaction with single excitations (CIS) calculations use a 6-31+G* basis and a restricted Hartree–Fock (RHF) reference determinant. They provide excitation energies from the ground electronic state to the relevant excited electronic states and reveal the similarities and differences between the Rydberg and valence electronic states in H_2O and H_2S.

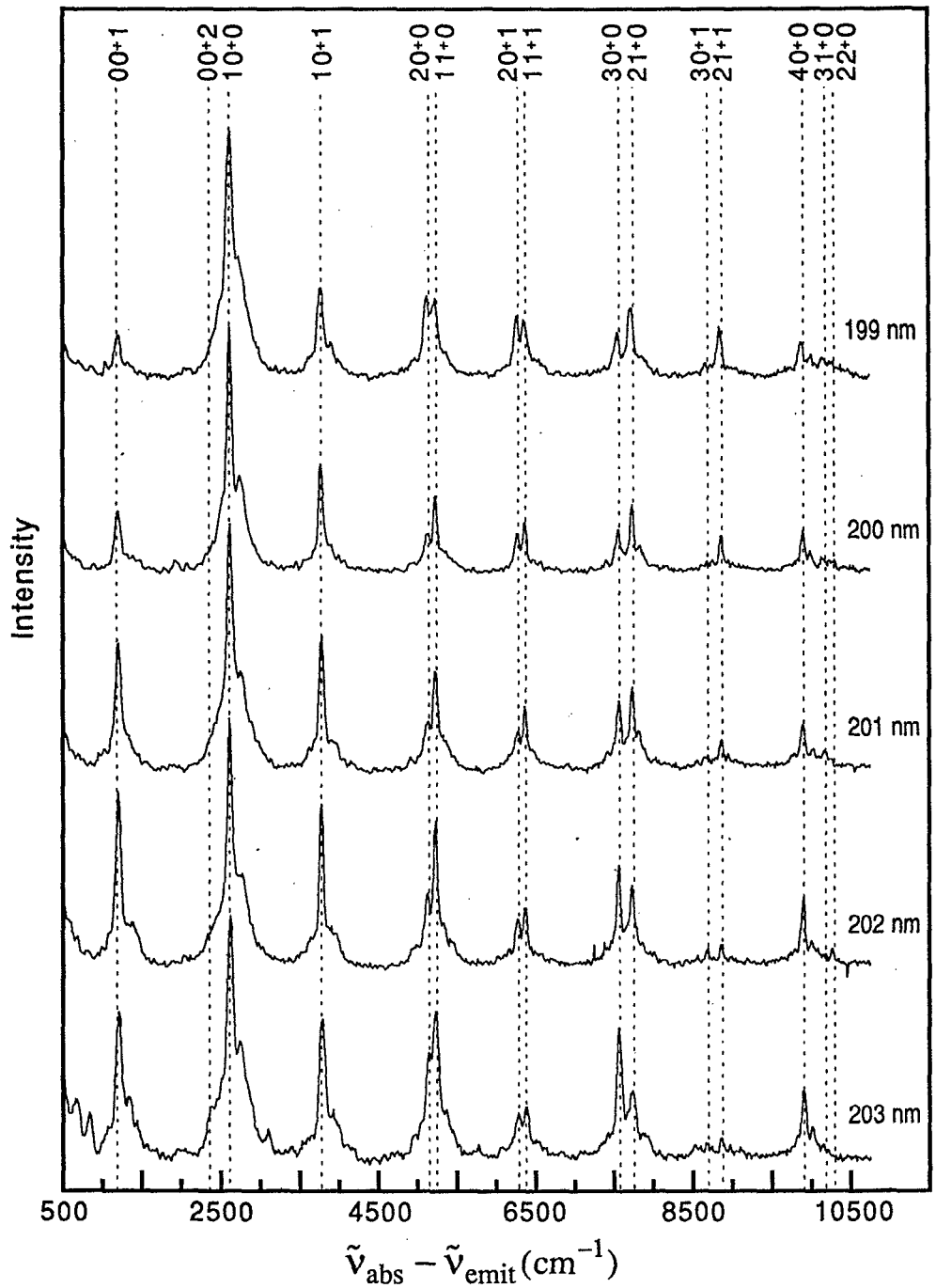

FIG. 1. Emission spectra of dissociating H_2S excited at 199 to 203 nm. Peaks are assigned according to a local mode basis, $(nm+b)$, where n=quanta in one SH oscillator, m=quanta in the other oscillator and b=quanta of bend. Dotted lines show predicted peak positions obtained from Ref. 28. Background scatter has been subtracted from the data, and each spectrum is multiplied by a constant in order to match the 10^+0 peak heights. OMA pixel to wave number calibration is determined with mercury lamp emission and fine tuned by matching the 10^+0 peak with the experimental value given in Ref. 28.

IV. RESULTS AND ANALYSIS

Figure 1 shows the emission spectra obtained for H_2S at five excitation wavelengths: 199, 200, 201, 202, and 203 nm. These spectra show emission into vibrational eigenstates in the ground state with from 500 to 11 000 wave numbers of vibrational energy, and Fig. 2 shows additional spectra at the 199 and 201 nm excitation wavelengths which include emission into higher vibrational eigenstates up to 16 500 wave numbers of energy. These spectra are assigned using a local mode basis to designate the final vibrational eigenstate[28] in the two-photon transition, with the zero point level in the ground electronic state taken as the initial state.[32] Some of the low-lying vibrational eigenstates closely resemble normal mode symmetric stretch wave functions, but at higher energies the vibrational eigenstates are best described in zeroth order in terms of a local mode representation.[29] For the

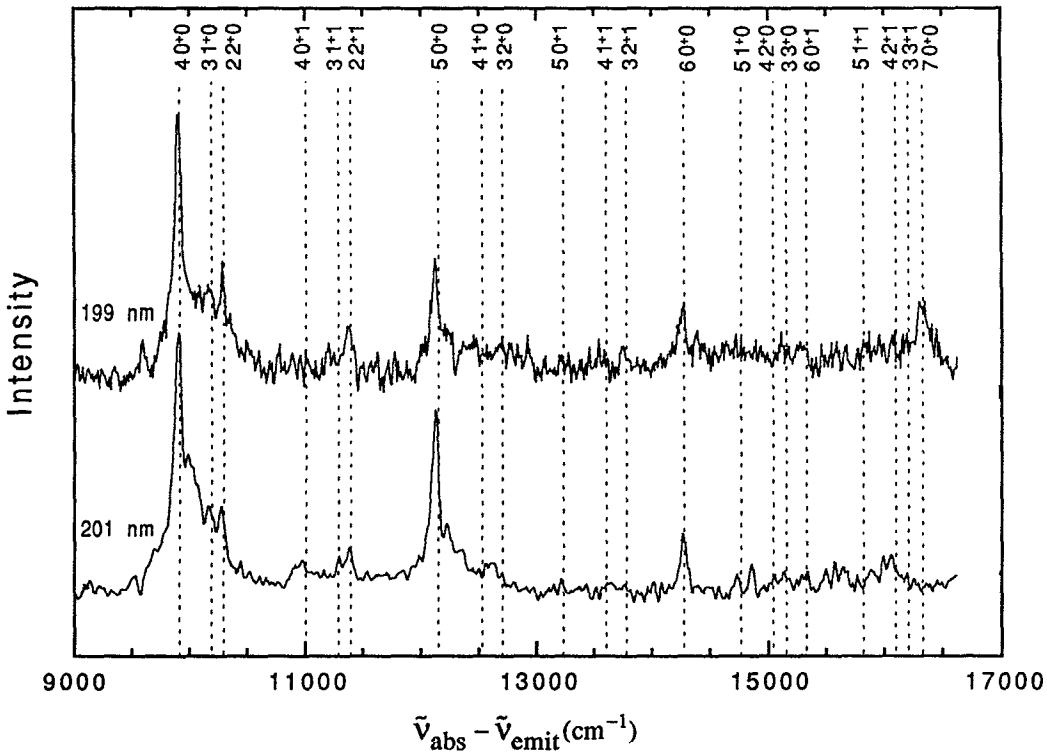

FIG. 2. Emission spectra at large Raman shifts for H_2S excited at 199 and 201 nm. Data is background subtracted and peak positions are calibrated as described in Fig. 1. The emission spectrum for excitation at 201 nm has been given a three point smooth. The region of this spectrum near 16 000 cm^{-1} shows some noise due to background scatter which could not be completely eliminated.

sake of consistency, local mode assignments are applied to the spectra, but Table I translates between the two assignments for comparison with previous spectra assigned in one or the other basis. To fully understand what dynamics are demonstrated by emission into a particular vibrational eigenstate, it is imperative to look at the actual vibrational eigenfunction, particularly since the assignment according to a particular basis set is not always an accurate indication of the actual spatial distribution of the wave function. We depict a few of the calculated[18] vibrational eigenfunctions of ground state H_2S in Fig. 3 to help in the interpretation of the emission spectra.

For both H_2O and H_2S at most excitation energies, the emission spectra are dominated by emission into the 10^+0, 20^+0 and 30^+0 vibrational eigenstates, consistent with a normal mode zeroth-order picture of these eigenstates as increasing quanta in the symmetric stretch. In the Franck–Condon region of the $^1B_1$ surface in H_2O and the bright $^1B_1$ surface in H_2S, the steepest gradient in the Franck–Condon region leads to outward motion in the symmetric stretch, so emission into a progression in the symmetric stretch is expected. The most striking aspects of the emission spectra presented here for H_2S in the excitation region between 199 and 203 nm, in comparison with the emission spectra at virtually every other excitation wavelength in the absorption band measured by Brudzynski *et al.* are that (1) emission into vibrational eigenstates with quanta in the bend is enhanced, and (2) emission into the 11^+0 is comparable to or greater than emission into 20^+0, as is emission into 21^+0 as compared to 30^+0. Clearly, outward motion in the symmetric stretch is not the only significant dynamics near the Franck–Condon region when one excites H_2S near 200 nm.

While there are dramatic differences in the emission to the low-lying vibrational eigenstates as one tunes the excitation wavelength, the emission into the highest vibrational eigenstates (Fig. 2) is dominated by the 40^+0, 50^+0, 60^+0, and 70^+0 bands, just as previously reported spectra at 193 nm excitation wavelength was dominated by the 60^+0 and 70^+0 bands later in the spectrum.[11] The dominance of these features is indicative of motion entirely different from the symmetric stretching motion associated with the lower energy $n0^+0$ modes. Emission to these higher energy $n0^+0$ modes corresponds to the stretching of a single SH bond as the molecule feels the dissociative forces of the exit channel. At these higher levels of vibration, the local mode $n0^+0$ assignments become increasingly accurate descriptions of the eigenstates as the vibrational motion is best characterized by oscillation in a single SH bond. The transition from emission to nm^+0 and nm^+b as well as $n0^+0$ modes in the spectra collected from 0 to 11 000 wave numbers (Fig. 2), to the dominance of $n0^+0$ in emission at greater than 11 000 wave numbers, demonstrates the evolution in the dynamics from the Franck–Condon region, where there is motion in both S–H oscillators and some bending, to purely dissociative motion of one S–H oscillator in the exit channel. This evolution in dynamics leads to the cold product vibrational

TABLE I. Vibrational mode assignments. Energies listed are those of the vibrational modes in the ground electronic state calculated by Halonen and Carrington (Ref. 28). Normal mode assignments are as follows: v_1=symmetric stretch, v_2=bend, and v_3=antisymmetric stretch. Local mode assignments are as follows: n=quanta in one S–H oscillator, m=quanta in the other oscillator, and b=quanta in bend (+symmetry only).

	Normal mode			Local mode		
Energy (cm^{-1})	v_1	v_2	v_3	n	m	b
1183.2	0	1	0	0	0	1
2355.0	0	2	0	0	0	2
2614.2	1	0	0	1	0	0
3777.9	1	1	0	1	0	1
5144.4	2	0	0	2	0	0
5243.4	0	0	2	1	1	0
6286.8	2	1	0	2	0	1
6384.1	0	1	2	1	1	1
7575.4	3	0	0	3	0	0
7753.6	1	0	2	2	1	0
8698.6	3	1	0	3	0	1
8875.3	1	1	2	2	1	1
9909.7	4	0	0	4	0	0
10 189.8	2	0	2	3	1	0
10 294.9	0	0	4	2	2	0
11 010.6	4	1	0	4	0	1
11 289.7	2	1	2	3	1	1
11 391.8	0	1	4	2	2	1
12 149.8	5	0	0	5	0	0
12 526.2	3	0	2	4	1	0
12 700.7	1	0	4	3	2	0
13 604.1	3	1	2	4	1	1
13 778.9	1	1	4	3	2	1
14 278.7	6	0	0	6	0	0
14 764.3	4	0	2	5	1	0
15 041.1	2	0	4	4	2	0
15 153.8	0	0	6	3	3	0
15 327.5	6	1	0	6	0	1
16 097.6	2	1	4	4	2	1
16 206.3	0	1	6	3	3	1
16 327.5	7	0	0	7	0	0

and rotational distribution seen in photofragment product distribution studies at all energies.[19–23] The anomalous variation in the emission spectra near 200 nm does not have a large effect on the exit channel dynamics; the emission spectra from 11 000 to 17 000 wave numbers for 199 and 201 nm are qualitatively the same. The emission to low energy eigenstates, however, is very different for these two wavelengths. It is the dynamics occurring near the Franck–Condon region, prior to dissociation along the exit channel, that lead to these dramatically varying spectra.

Since the spectra span excitation wavelengths from the peak of the $v=0$ resonance in the absorption spectrum to one near the valley between the $v=0$ and $v=1$ features, one can easily assess whether the distinctive features in the emission attributed to initial motion near the Franck–Condon region are associated with being tuned to a symmetric stretch resonance or not. Clearly the enhancement of emission into vibrational eigenstates with quanta in the bend and the shift of the $20^+0/11^+0$ and $30^+0/21^+0$ emission intensity ratios in the direction of 11^+0 and 21^+0 both persist throughout this whole wavelength region; it does not come and go as one tunes the excitation energy through the absorption resonance. Furthermore, these features are unique to this region of the absorption profile and do not reappear near other resonance peaks. Later in this section and in the discussion section we refer to recent calculations of Heumann and Schinke[18] that show that emission into the 11^+0 and 21^+0 features is enhanced when the dynamics samples coupled regions of the bright $^1B_1$ and dark $^1A_2$ potential surfaces. Thus, the fact that the conical intersection between these two surfaces occurs near the Franck–Condon region at an excitation energy close to 200 nm explains why this nonadiabatic dynamics is evidenced preferentially in the emission to lower energy vibrational eigenstates upon excitation at 200 nm. In the next paragraph we use simple electronic structure calculations to analyze the nature of the $^1B_1$ and $^1A_2$ electronic configurations in the Franck–Condon region and consider how their interaction leads to the observed emission. This analysis suggests that for dynamics that propagate on a potential surface dominated by the $^1A_2$ electronic configuration, the electronic character generates a loosening of the potential in the bend angle and motion in the asymmetric stretching motion, consistent with our observed emission spectra near the conical intersection.

Our GAUSSIAN 92 calculations are in qualitative agreement with the higher level calculations of Schinke and coworkers and help reveal how the electronic character at various geometries lead to the observed spectra. In H_2S, unlike in H_2O, there are two electronic states in C_{2v} geometry in the region of interest: a dark dissociative state of $^1A_2$ symmetry and, at slightly higher energy, a bright state of $^1B_1$ symmetry which has predominantly bound Rydberg electronic character. Table II shows the nature of the molecular orbitals contributing to the states in C_{2v} geometry for H_2O and H_2S, as well as in the exit channel for H_2S. The $^1B_1$ and $^1A_2$ states reached in the first absorption band in these two molecules are formed by excitation to molecular orbitals of either a_1 or b_2 symmetry from a b_1 symmetry nonbonding molecular orbital, closely resembling a sulfur p orbital oriented perpendicular to the molecular plane (see Fig. 4). Note that while, in water, the excited orbital in the $np_y(b_1) \rightarrow (n+1)s/\sigma^*(a_1)$ transition to the $^1B_1$ electronic state has mixed Rydberg/valence character in the Franck–Condon region as shown in Table II, in H_2S the excited orbital in the transition to the $^1B_1$ electronic state, shown in Table II and in Fig. 4, is primarily Rydberg in character (there is a small contribution, not shown in Table II, to the electronic state from another $(b_1) \rightarrow (a_1)$ transition with a bit of valence character). The valence electronic character in H_2S appears in the excited orbital of the $^1A_2$ state, a b_2 symmetry orbital which is antibonding in the SH stretching coordinates (Fig. 5). (In the Franck–Condon region, the lowest $^1A_2$ state in water is two electron volts higher in energy than the $^1B_1$ state so does not contribute to the dynamics upon photodissociation in the first absorption band.) Thus it is clear why models of H_2O refer to a dissociative $^1B_1$ surface, while model of H_2S photodissociation invoke a dissociative $^1A_2$ state and designate the $^1B_1$ state as bound. However, upon breaking symmetry from C_{2v} to C_s, (caused by motion along the antisymmetric stretch coordinate) these states correlate to the same symmetry, A'', and evidence a mixed Rydberg/valence

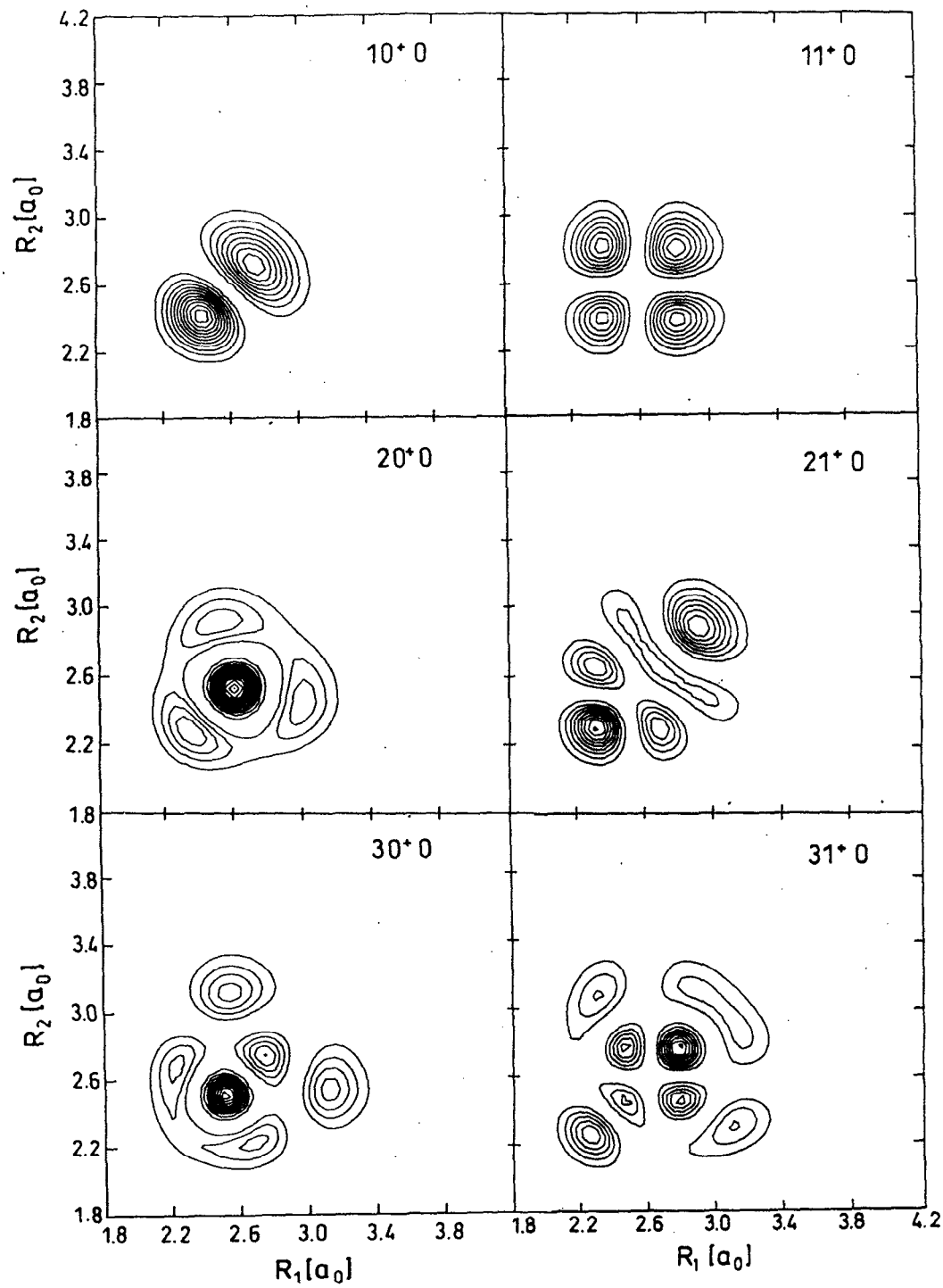

FIG. 3. Calculated ground state vibrational eigenfunctions of H_2S adapted with permission of the authors from Ref. 18.

electronic character. The upper orbital in the dominant electronic configuration contributing to the electronic wave function at molecular geometries in the exit channel has considerable antibonding character along the S–H bond that is stretched (Fig. 5); one can see how a linear combination of the two locally antibonding molecular orbitals in the two exit channels gives a valence orbital that looks like the excited b_2 orbital in the $^1A_2$ electronic state. Although the dissociative electronic state is described as optically dark in the dynamics calculation of Heumann and Schinke,[18] those calculations are done in a diabatic representation of the states; the dissociative adiabatic potential energy surface is not optically dark. Our calculations show that the bright character of the Rydberg electronic configuration (which would characterize a

TABLE II. Molecular orbitals in the 6-31+G* basis making the largest contributions to the electronic transitions in H_2O and H_2S, as calculated by GAUSSIAN 92. Results are tabulated for both molecules at equilibrium geometry (<HSH=92.2°, $R(S-H)_{equil.}=1.3384$ Å; <HOH=104.5°, $R(O-H)_{equil.}=0.958$ Å) and for H_2S with either S–H bond stretched to 4.0 Å, leaving the other bond fixed. The molecules are oriented in the XZ plane with the oxygen/sulfur atom at the origin, one O/S–H bond oriented to place the hydrogen atom (H_1) on the positive Z axis and the other S–H bond oriented to place the second hydrogen atom (H_2) near the positive X direction. The $^1B_1$ Rydberg/dissociative electronic configuration for H_2O involves an excitation from the np_y orbital to the $(n+1)s/\sigma^*$ orbital. The density in S-type orbitals centered on the oxygen atom demonstrates Rydberg character, but the density of opposite phase on the hydrogen atoms lead to some OH antibonding character. Note that in H_2S, the $^1B_1$ electronic configuration has predominantly Rydberg character; the $(n+1)s$ orbital is almost entirely centered on the sulfur atom, and lacks the dissociative character of the corresponding Rydberg transition in H_2O. The $^1A_2$ dissociative state for H_2S is formed by the excitation from the np_y orbital to the σ^* orbital. These calculations were used to generate the pictures of the molecular orbitals shown in Figs. 4 and 5. The calculations at stretched geometries show the antibonding components in the individual SH bonds which mix at equilibrium to give the σ^* orbital responsible for the dissociative character for H_2S. These orbitals are shown in Fig. 5.

		H_2O		H_2S			Exit Channel (H_2S)	
		$np_y(b_1)$	$(n+1)s/\sigma^*(a_1)$	$np_v(b_1)$	$\sigma^*(b_2)$	$(n+1)s(a_1)$	Stretch SH_1	Stretch SH_2
O/S	1S		0.08068			−0.01823	−0.00271	−0.00271
	2S		−0.04755			0.11009	0.01297	0.01297
	2PX		0.12739		−0.10428	0.03693	0.00251	***0.17559***
	2PY	***0.63893***		***−0.25904***				
	2PZ		−0.09864		0.10837	0.03554	***0.17562***	−0.00424
	3S		***−0.95544***			−0.12151	−0.02686	−0.02686
	3PX		−0.15630		***0.27556***	−0.10136	−0.00746	***−0.45735***
	3PY	***0.46547***		***0.69276***				
	3PZ		−0.12102		***−0.28635***	−0.09754	***−0.45740***	0.01010
	4S					***−1.05538***	−0.04231	−0.04231
	4PX				***0.84752***	−0.16563	0.01160	***−0.33073***
	4PY			***0.41901***				
	4PZ				***−0.88070***	−0.15939	***−0.33142***	0.02431
	S		***1.84724***			***1.53753***	0.08544	0.08544
	PX		***0.57162***		−0.13412	***0.27962***	0.00297	−0.00542
	PY	0.08218		0.03663				
	PZ		***0.44260***		0.13937	***0.26908***	−0.00554	0.00318
	XX		0.04489		−0.09555	0.00511	−0.00083	0.00359
	YY		0.06014			0.02190	−0.00186	−0.00186
	ZZ		0.04592		0.09555	0.00524	0.00425	−0.00017
	XY	0.02646		0.01324				
	XZ		−0.00229		0.00424	−0.00195	−0.00986	−0.01005
	YZ	0.02048		0.01274				
H_1	1S		0.05237		0.14106	0.02250	***0.24140***	0.00360
	2S		***−0.35401***		***1.04138***	0.05362	***0.54314***	−0.02619
H_2	1S		0.05237		−0.14106	0.02250	0.00360	***0.24140***
	2S		***−0.35401***		***−1.04138***	0.05362	−0.02619	***0.54314***

$^1B_1$ diabat) lends some brightness to both the dissociative and the bound adiabats in non-C_{2v} geometries in the exit channel. We obtained oscillator strengths for H_2S with one bond stretched or both bonds symmetrically stretched to enable us to compare the oscillator strength for an optical transition to a geometry on the bound adiabat where $^1B_1$ symmetry was maintained vs a geometry in the exit channel on the dissociative adiabat with mixed electronic character. These displaced geometries correspond to regions where the potential energy difference between the ground state and excited state had decreased to that corresponding to the latter part of our emission spectra. For the geometry along the symmetric stretch coordinate with both bonds stretched to 1.6 Å, the oscillator strength for the $^1B_1$ state was $f=0.0155$. For the geometry in the exit channel with one bond at the ground state equilibrium value of 1.3384 Å and the other stretched to 1.55 Å, the oscillator strength between the lower dissociative adiabat and the ground state was, $f=0.008$. So, while the dissociative state is rigorously dark in C_{2v} geometry, it has considerable bright character at geometries further along the dissociative coordinate permitting us to be optically sensitive to the exit channel dynamics. In the dynamics calculations of Heumann and Schinke[18] done in an approximately diabatic representation one can see the dynamics generated by the dissociative valence electronic character characterizing the $^1A_2$ diabat[33] when it mixes, due to off diagonal potential coupling, to the diabatic $^1B_1$ surface. Figure 6 shows contour plots depicting the time-dependent propagation of a wave packet projected onto the diabatic $^1B_1$ surface. The wave packet experiences strong initial forces along the symmetric stretch coordinate, but very quickly starts to spread toward the exit channels. At 4.8 fs the wave packet has significant amplitude in the exit channels, where this nuclear motion in the antisymmetric stretch toward the exit channels is generated by motion on the diabatic surface resulting from the valence electronic configuration (which is $^1A_2$ in C_{2v}) but is spectroscopically visible due to the Rydberg character ($^1B_1$ in C_{2v}) of molecules sampling significant displacements along the adiabatic dissociative coordinate.

The *ab initio* surfaces generated by Schinke and co-workers,[16] along with the orbital information extracted from our Gaussian calculations, reveal the nature of the

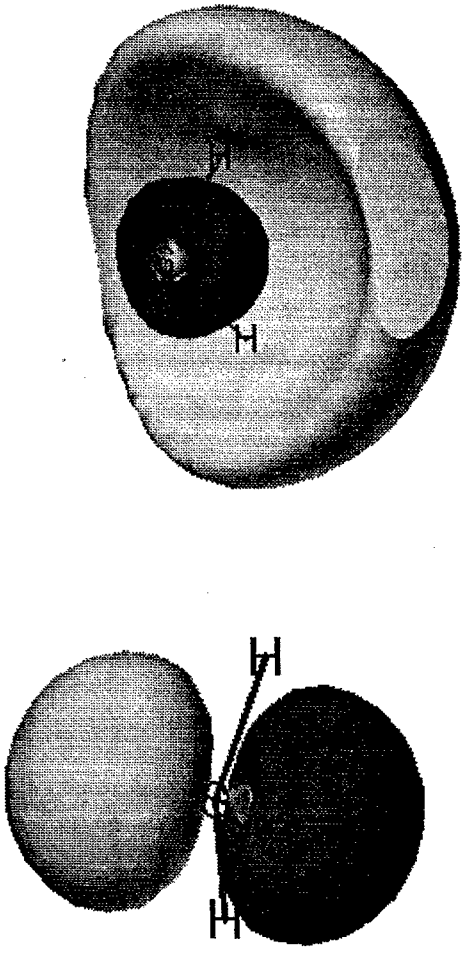

FIG. 4. Molecular orbitals contributing to the bound surface in H_2S ($^1B_1$ in C_{2v}). This surface is formed by excitation from a nonbonding orbital, closely resembling a sulfur p orbital (bottom) to a Rydberg-like orbital (top). There is also a small valence contribution from excitation to an orbital (not shown) which is antibonding along the symmetric stretch coordinate. Orbitals were tabulated for visualization on a CAChe Scientific, Inc. workstation, Version 3.5.

forces acting on the photoexcited molecule. The initial forces are along the symmetric stretch coordinate for the $^1B_1$ and $^1A_2$ states, but also along the dissociative antisymmetric stretch coordinate for the $^1A_2$ state. The high level calculations of Schinke and co-workers also indicate that the $^1B_1$ state has a minimum in the bend coordinate at roughly the same geometry as the ground state, while in contrast the $^1A_2$ state is flat along the bend coordinate and shows no clear minimum. Therefore, the $^1B_1$ character of the surface will lead to symmetric stretching motion with little variation in the bend angle and the valence ($^1A_2$ in C_{2v}) character of the dissociative surface will lead to asymmetric stretching motion and the flatness along the bend coordinate will cause a loosening of the molecular bend angle. Thus, we assign the enhancement of emission into vibrational eigenstates with quanta in the bend and the shift of the $20^+0/11^+0$ and $30^+0/21^+0$ emission intensity ratios in the direction of 11^+0 and 21^+0 to dynamics near the conical intersection with the dissociative surface. Indeed, Heumann and Schinke's calculations show a second maximum in the time dependent overlap of the dissociating wave packet with the 11^+0 and 21^+0 states near 4.8 fs, just when Fig. 6 shows amplitude beginning to enter the dissociative exit channel.

V. DISCUSSION

The first ultraviolet absorption bands of both H_2O (Ref. 10) and H_2S (Refs. 6 and 7) are broad continua with diffuse superimposed structure assigned to resonances in the symmetric stretch; in H_2S the absorption band extends from 170 to 230 nm with the broadened symmetric stretch resonance features beginning at about 200 nm and extending to the blue. Schinke and co-workers[17] describe the symmetric stretch structure differently for the two systems, stating that in H_2O the symmetric stretch resonances are a consequence of motion on the rim of the dissociative potential energy surface while in H_2S they are due to symmetric stretch motion at the bottom of a $^1B_1$ potential surface that is binding, not dissociative, in their diabatic representation. This interpretation is based on three-dimensional surfaces which place the $^1B_1$ diabatic surface at higher energies than the $^1A_2$ surface in the Franck–Condon region. In their best calculations,[16] however, the $^1B_1$ potential energy surface is in fact lower than the $^1A_2$ potential energy surface in the Franck–Condon region, so the lower dissociative adiabat of H_2S has $^1B_1$ character here. Thus, in both H_2O and H_2S the symmetric stretch motion originates on a lower dissociative adiabatic potential energy surface which has $^1B_1$ character in the Franck–Condon region. In fact, the striking similarities in the absorption spectrum and the emission spectra at most energies are entirely consistent with the isoelectronic nature of these two molecules. In this paper, however, we will focus on the differences between these two very similar molecules. While in H_2O the dissociative portion of the potential energy surface results from a valence electronic configuration which has $^1B_1$ character in C_{2v} geometries, in H_2S the $^1B_1$ electronic configuration is dominated by Rydberg character, and the dissociative character comes from an excited electronic configuration which has $^1A_2$ symmetry in C_{2v} (see Table II). Schinke and co-workers' best calculation shows that at the ground state equilibrium HSH angle of 92.2 deg, the $^1A_2$ potential intersects the $^1B_1$ potential at two points along the symmetric stretch coordinate, one close to the Franck–Condon region at slightly longer S–H symmetric stretch geometries than the ground state equilibrium and one at 0.9 atomic units further out, at the outer turning point side of the potentials. The inner crossing leads to a conical intersection of the resulting adiabats within the region of the surface vertically accessed in our energy range near 200 nm. It is the strong mixing in of $^1A_2$ character in the region of this conical intersection which leads to the dramatically different emission spectra obtained in this energy region.

Reviewing the emission spectra of H_2O facilitates the interpretation of the similar spectra for H_2S as well as highlights the differences between the two molecules. The emission spectra for H_2O are qualitatively reproduced by the dynamics calculations of Schinke and co-workers[10] on *ab initio* surfaces, and can be understood when one also carefully examines the ground state vibrational wave functions for H_2O.

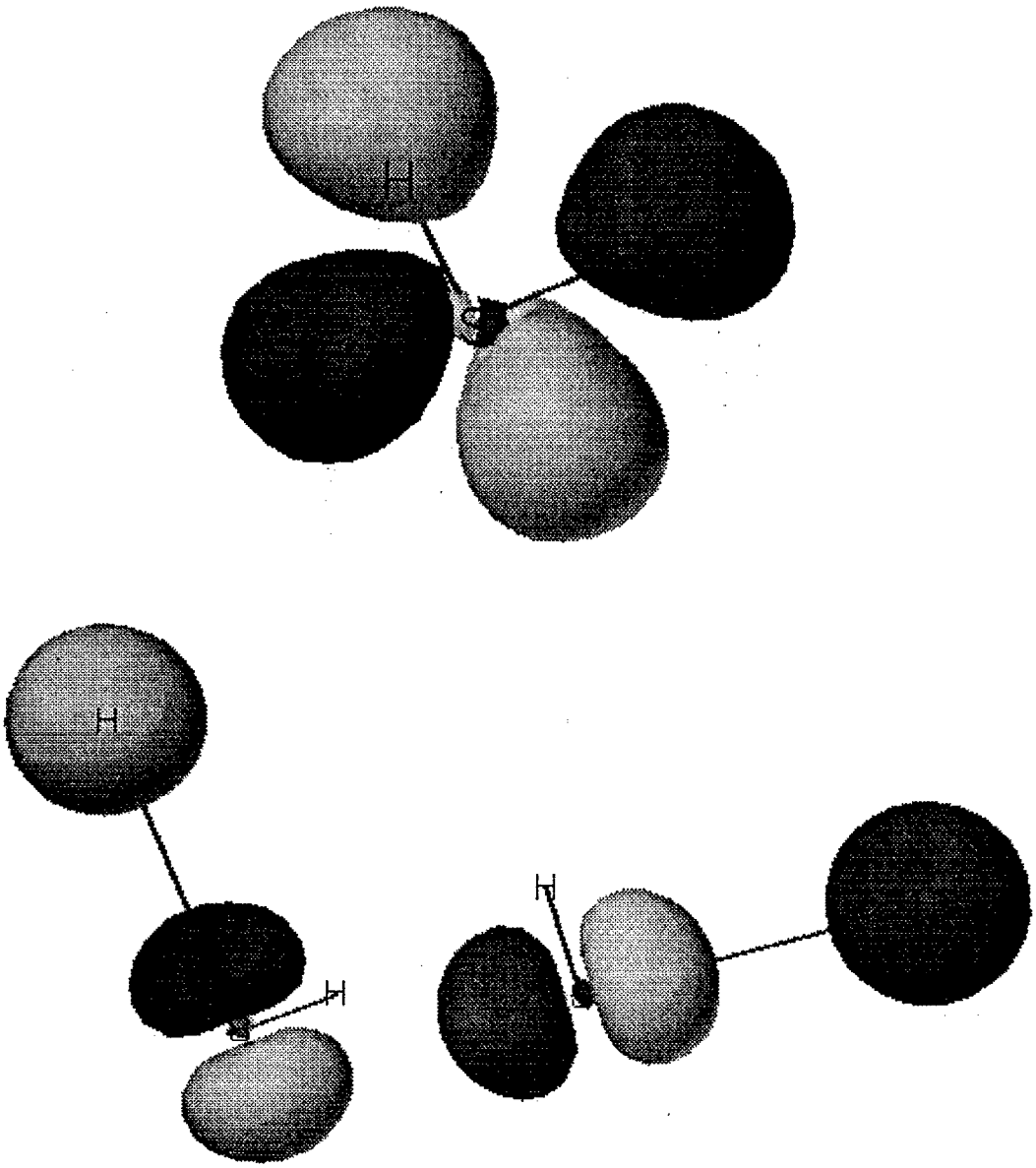

FIG. 5. Molecular orbital contributing to the dissociative surface ($^1A_2$ in C_{2v} geometries) for H_2S. This surface is formed by excitation from a nonbonding molecular orbital centered on the sulfur (shown in Fig. 4) to this antibonding orbital (top). This orbital is formed from a linear combination of two antibonding orbitals localized on either S–H oscillator (bottom). These localized antibonding orbitals depicted on the bottom were generated by stretching either S–H bond to 4.0 Å to demonstrate the S–H antibonding character of the stretched bond in the exit channel. At equilibrium geometries, these localized orbitals mix to form the resultant orbital shown above (top). Orbitals were tabulated for visualization on a CAChe Scientific, Inc. workstation, Version 3.5.

Roughly identical emission spectra for H_2O were obtained by Hudson and co-workers at several wavelengths in the first absorption band.[34] The emission to the 20^+0 and 30^+0 modes is much stronger than that to the 11^+0 and 21^+0 modes, while the 40^+0 and 31^+0 modes are of nearly equal intensity. The spectrum shows a trend of early dominance of $n0^+0$ with a gradual increase in emission to nm^+0 modes. This is consistent with Schinke and co-workers' description of the dynamics. The initial forces on the molecule are along the symmetric stretching coordinate. For small amounts of vibrational motion, normal mode symmetric stretch motions are good descriptions of the 10^+0 and 20^+0 eigenstates. With larger amounts of vibrational motion, however, this type of normal mode motion is no longer a good description of the $n0^+0$ eigenstates.[29] Therefore larger amplitudes of symmetric stretching motion will not solely overlap the $n0^+0$ eigenstates at high n, as these are closer to local mode stretching eigenstates; emission into both $n0^+0$ and nm^+0 eigenstates is then observed. The emission spectra for H_2S are interpreted similarly, yet there are additional complications due to the strong mixing in the vicinity of the conical intersection.

The emission spectra for H_2S demonstrate dynamics that

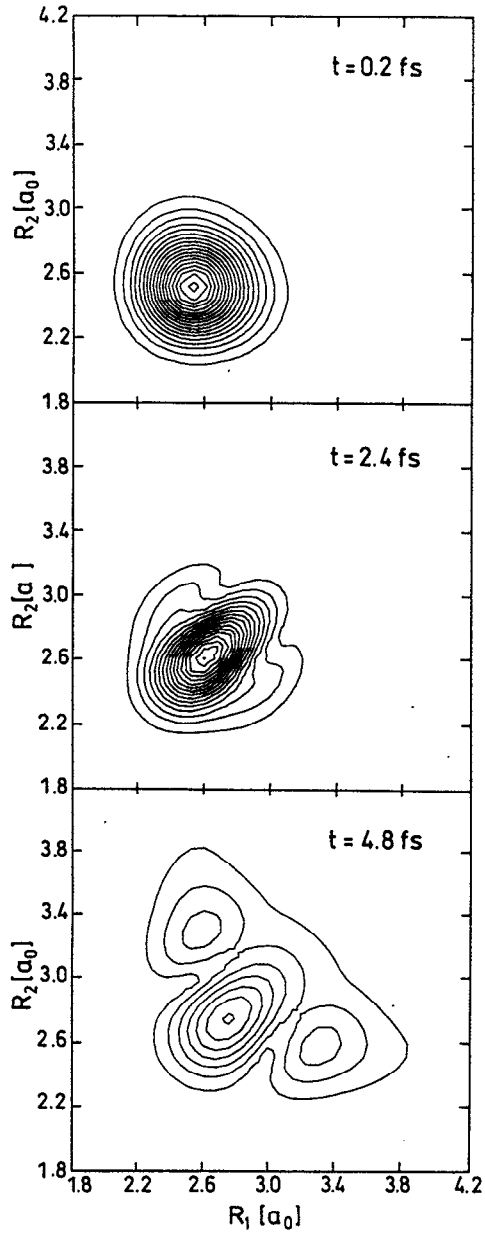

FIG. 6. Contour plots depicting the time-dependent propagation of a wave packet on an approximately diabatic $^1B_1$ surface. Figure reproduced with permission of the authors from Ref. 18.

sample the conical intersection. This sampling will occur at earlier or later times in the dissociation dynamics depending on the proximity of the intersection to the region of the surface accessed by vertical excitation. Emission spectra reported by Hudson and co-workers[15] on the blue side of the absorption profile correspond to excitation to a region of the surface dominated by $^1B_1$ electronic character, and therefore can be partially understood using the same interpretation as for H_2O. Excitation at these wavelengths will access a region of the potential surface significantly displaced from the minimum of the $^1B_1$ surface along the symmetric stretch coordinate. The initial forces will be along the symmetric stretching coordinate, and as with H_2O, these dynamics will lead to overlap with $n0^+0$ states for small displacements and with both $n0^+0$ and nm^+0 states at larger displacements. As the dynamics evolve, the classical molecular trajectory samples geometries at larger displacements along the symmetric stretch coordinate and passes through the region of the conical intersection as it nears the minimum of the $^1B_1$ surface. As regions of the surface with significant $^1A_2$ character are sampled near the conical intersection, the molecule will feel forces along the dissociative coordinate and experience a flatter bend potential. This leads to the inclusion of emission to modes involving low amplitude bending motion and further enhancement of nm^+0 modes in the later portion of the spectrum. As one tunes the excitation wavelength to the red, vertical excitation accesses a region of the surface closer to the conical intersection of the $^1A_2$ and the $^1B_1$ surfaces. The dissociating amplitude will sample the conical intersection earlier, so the features associated with this region of the surface appear in emission to lower energy ground state vibrational eigenstates. This is because, in a semiclassical picture, emission from a dissociating molecule is dependent on good Franck–Condon overlap with ground vibrational eigenstates in both position and momentum. Dynamics associated with a certain region of the potential energy surface will be observed in the emission to higher energy eigenstates for higher excitation energies because the dissociating molecule will have a larger momentum when sampling the same region of the surface.[35] In the spectra obtained by Hudson and co-workers at 188 and 192 nm as well as that of Butler and co-workers at 193 nm, there is certainly an enhancement of the nm^+0 and nm^+b features in the later part of the spectra. These features appear earlier in the emission spectra for redder excitation wavelengths.

The emission spectra reported in this paper, in the range 199 to 203 nm, correspond to vertical excitation energies which access regions of the surface near the conical intersection. With significant mixing in of $^1A_2$ character, the molecule accesses the conical intersection early in its motion and feels significant initial forces along the antisymmetric dissociative coordinate as well as a loosening of the bend angle. This effect appears in the first few peaks in the spectra as there is preferential overlap with the 11^+0 and 21^+0 vibrational eigenstates as well as strong enhancement of the bending fundamental. For example, the 11^+0 eigenstate, best viewed in a local mode representation (Fig. 3), has amplitude at geometries accessed by dissociative motion in the antisymmetric stretch. This dynamics was first indicated by the time dependent calculations of Heumann and Schinke,[18] done in an approximate diabatic representation; the calculations showed that portions of the dissociating wave packet which head out along the antisymmetric stretch dissociative coordinate and retain some optically bright $^1B_1$ diabatic character give emission to the 11^+0 and 21^+0 bands, as observed in our spectra. In comparing our spectra with the calculated results, we note that the emission spectra should show the emission to 11^+0 growing in and eventually dominating the 20^+0 mode only at energies that correspond to vertical excitations near the conical intersection. As explained above, if the earliest dynamics sample the conical intersection, the ef-

fects of mixing in of $^1A_2$ character should appear in emission to the lowest energy vibrational eigenstates. One can see this effect in our spectra shown in Fig. 1; tuning the excitation energy through the conical intersection causes a shift in the intensity of the modes involving one quantum of bend and evidencing dissociative motion (11^+0 and 21^+0) to lower vibrational eigenstates as the dynamics samples the conical intersection closer to the region accessed via vertical excitation. As we tune the excitation wavelength from 199 to 203 nm, we see the anomalous intensity in these modes shift to earlier in the spectrum. Referring to Fig. 1, one can see that at 199 nm the 21^+1 peak is clearly present, the 21^+0 peak has greater intensity than 30^+0, the 20^+0 and 11^+0 peaks have similar intensities, and the 10^+1 has greater intensity than a very small 00^+1 peak. At 201 nm the 21^+1 peak is much smaller, the 21^+0 and 30^+0 peaks have nearly equal intensities, the 11^+0 is much larger than the 20^+0 peak, and the 10^+1 and the 00^+1 peaks are much larger and nearly equal in size. Finally, at 203 nm, the 21^+1 peak is gone, the 30^+0 is much larger than the 21^+0 peak, the 11^+0 and 20^+0 peaks are getting closer in size, and the 10^+1 and 00^+1 peaks are still large and equal in size. This dramatic variation in this wavelength range allows us to identify this region vertically accessed at these energies as that of the conical intersection. In the calculations of Heumann and Schinke, they see an analogous effect in the wavelength dependence of the calculated emission intensity into the 11^+0 and 21^+0 eigenstates. However, as their calculations are done using their less accurate potential energy surfaces, the conical intersection is at higher energies than 200 nm, so the peak in the predicted 11^+0 emission intensity occurs at excitation wavelengths to the blue of our observed spectra.

Excitation at wavelengths even further to the red, such as those reported by Hudson for excitations at 209, 218, and 223 nm, access a region of the surface past the conical intersection, and these features associated with $^1A_2$ character begin to disappear from the spectra. The spectra reported at 218 and 223 nm are so far to the red of the absorption maximum that resonant vertical excitation at these energies should directly access the exit channel of the dissociative surface. This very weak resonant excitation should yield minimal emission and the spectra collected at these wavelengths are likely to be dominated by off resonance Raman contributions.

Understanding how the excitation energy affects where in the S–H emission progression a particular feature of the dissociation dynamics is manifest also helps clarify our identification of the emission into the high energy $n0^+0$ states as indicative of exit channel dynamics in H_2S. The spectra near 200 nm show complicated emission to $n0^+0$, nm^+0, and nm^+b modes in the early portion of the spectra which evolve towards eventual dominance by $n0^+0$ modes in the later part of the spectra. At 193 nm, only the emission far out at 60^+0 and 70^+0 evidenced the pure single bond stretching motion in the exit channel.[9,11] Even the emission bands with five quanta in the stretch showed significant contributions from the nm^+0 and nm^+b modes. We can understand this by noting that excitation at high energies in the absorption profile will access regions well up from the minimum of the $^1B_1$ surface along the symmetric stretch coordinate, and therefore the initial forces on the molecule will generate significant momentum and displacement along the symmetric stretch coordinate in the early part of the dynamics. This high energy symmetric stretch motion will generate overlap with highly excited vibrational eigenstates, giving emission into both nm^+0 and $n0^+0$ states. Additionally, as the dissociating molecule samples the conical intersection, the influence of the $^1A_2$ surface leads to emission to nm^+1 modes. These factors contribute some emission to nm^+0 and nm^+b states which appear in conjunction with the more dominant $n0^+0$ modes associated with exit channel dynamics. At the lower excitation energy corresponding to 200 nm, however, the dynamics from the early symmetric stretching motion and the conical intersection result in the emission into only the low-lying vibrational eigenstates, and the latter part of the spectrum is dominated by emission into 40^+0, 50^+0, etc. states characteristic of the same exit channel dynamics that appeared in the 60^+0 and 70^+0 emission at 193 nm.

The *ab initio* calculations of Schinke and co-workers and the emission spectra reported in this paper indicate the presence of a conical intersection in the region of the surface vertically accessed at about 200 nm. We now examine how vertical excitation to the region of the conical intersection influences the photofragment vibrational and rotational product distributions. The dissociation of H_2S at all energies results primarily in vibrationally and rotationally cold SH fragments.[19–23] Reanalysis of the comprehensive study by Xie *et al.*,[23] however, reveals a fascinating anomaly in the SH vibrational distribution. Their photofragmentation experiments encompassed 14 different wavelengths, including several in the vicinity of 200 nm. (Previous studies had relied on excimer wavelengths or 266 nm from a quadrupled Nd:YAG and had not examined this particular region of the spectrum.) At wavelengths near 200 nm the fraction of SH fragments produced in their vibrational ground state jumps dramatically with small drops in energy available to the recoiling fragments. The percentage of SH fragments in the vibrational ground state rises from 61.3% at 199.76 nm excitation to 80.3% at 203 nm excitation. This is a nearly 20% increase in $v=0$ SH products with only a 4% drop in the available energy. The $v=0$ SH products are preferentially formed when the early dynamics in the Franck–Condon region are in the direction of the dissociative coordinate in H_2S and therefore the recoiling SH fragment is left with very little vibrational excitation. As the vertically accessed region of the electronic surface becomes dominated by $^1A_2$ character the initial forces evolve from those along the symmetric stretching coordinate to those along the dissociative coordinate, and this evolution is reflected in the fragmentation product distribution. This dramatic change over such a short energy interval is indicative of the rapidly changing character of the dissociative surface and provides additional evidence of a conical intersection in the region of the surface sampled at these excitation energies.

Note added in proof. J. Svitak, J. Rose, N. Bannas, and M. Kellman (private communication) have recently analyzed the dynamical character of the vibrational eigenstates of H_2S by calculating the corresponding classical trajectories on a phase sphere. Their calculated separatrix energies divide

each polyad of eigenstates into two sets, those states best described as normal modes and those best described as local modes. The separatrix energies and their classical trajectory plots and quantum wave functions obtained within a two oscillator model (which fits the experimentally determined eigenstate energies) confirm the local mode character of the eigenstates $n0^{+}0$ with $n=5,6,7$ observed in the latter part of our emission spectra.

ACKNOWLEDGMENTS

This work was supported by the Division of Chemical Sciences, Office of Basic Energy Sciences, Office of Energy Research, U.S. Department of Energy, under Grant Nos. DE-FG02-92ER14305 (Butler) and W-31-109-ENG-38 (Hessler). L.J.B. gratefully acknowledges the support of a Camille and Henry Dreyfus Foundation Teacher-Scholar Award and an Alfred P. Sloan Research Fellowship. We thank R. Schinke and co-workers for providing us with some of the figures from their work in Ref. 18 prior to publication. We thank D. C. Kitchen in our group for his essential help in generating the figures of molecular orbitals in this paper.

[1] See, for example, review by D. E. Manolopoulos, K. Stark, H. Werner, D. W. Arnold, S. E. Bradforth, and D. M. Neumark, Science **262**, 1852 (1993).

[2] See A. Kuppermann and Y.-S. Mark Wu, Chem. Phys. Lett. **205**, 577 (1993), and extensive references within.

[3] M. Born and R. Oppenheimer, Ann. Phys. **84**, 457 (1927).

[4] For one of the best early reviews of nonadiabatic molecular collisions, see J. C. Tully in *Dynamics of Molecular Collisions Pt. B*, edited by W. H. Miller (Plenum, New York, 1976), p. 217.

[5] For some recent work from our laboratory, see P. W. Kash, G. C. G. Waschewsky, L. J. Butler, and M. M. Francl, J. Chem. Phys. **99**, 4479 (1993); P. W. Kash, G. C. G. Waschwesky, R. E. Morss, L. J. Butler, and M. M. Francl, *ibid.* **100**, 3463 (1994).

[6] L. C. Lee, X. Wang, and M. Suto, J. Chem. Phys. **86**, 4353 (1987).

[7] K. O. Lantz and V. Vaida, Chem. Phys. Lett. **215**, 329 (1993).

[8] Another example where photoexcitation of a molecule, CH_3SH, provided Franck–Condon access to the transition state region of an excited state reaction coordinate ($CH_3+SH \rightarrow CH_3S+H$) is in E. Jensen, J. S. Keller, G. C. G. Waschewsky, J. E. Stevens, R. L. Graham, K. F. Freed, and L. J. Butler, J. Chem. Phys. **98**, 2882 (1993).

[9] L. J. Butler, Chem. Phys. Lett. **182**, 393 (1991).

[10] See V. Engel, V. Staemmler, R. L. VanderWal, F. F. Crim, R. J. Sension, B. Hudson, P. Andresen, S. Hennig, K. Weide, and R. Schinke, J. Phys. Chem. **96**, 3201 (1992), and references within.

[11] For the emission spectrum of H_2S excited at 193.3 nm and for the first discussion of reassigning the structure in the absorption spectrum to symmetric stretching states, see M. D. Person, K. Q. Lao, B. J. Eckholm, and L. J. Butler, J. Chem. Phys. **91**, 812 (1989).

[12] For one of the better descriptions of the structure in the absorption spectrum of H_2O, see N. E. Henriksen, J. Zhang, and D. G. Imre, J. Chem. Phys. **89**, 5607 (1988).

[13] R. T Pack, J. Chem. Phys. **65**, 4765 (1976).

[14] E. J. Heller, J. Chem. Phys. **68**, 3891 (1978).

[15] R. J. Brudzynski, R. J. Sension, and B. Hudson, Chem. Phys. Lett. **165**, 487 (1990).

[16] K. Weide, V. Staemmler, and R. Schinke, J. Chem. Phys. **93**, 861 (1990). See also earlier work by G. Theodorakopoulos, I. D. Petsalakis, and C. A. Nicolaides, Chem. Phys. Lett. **207**, 321 (1993), and references within.

[17] B. Heumann, K. Weide, R. Düren, and R. Schinke, J. Chem. Phys. **98**, 5508 (1993).

[18] B. Heumann, and R. Schinke, J. Chem. Phys. (in press).

[19] G. N. A. Van Veen, K. A. Mohamed, T. Baller, and A. E. De Vries, Chem. Phys. **74**, 261 (1983).

[20] R. E. Continetti, B. A. Balko, and Y. T. Lee, Chem. Phys. Lett. **182**, 400 (1991).

[21] Z. Xu, B. Koplitz, and C. Wittig, J. Chem. Phys. **87**, 1062 (1987).

[22] B. R. Weiner, H. B. Levene, J. L. Valentini, and A. P. Baronavski, J. Chem. Phys. **90**, 1403 (1989).

[23] X. Xie, L. Schneider, H. Wallmeier, R. Boettner, and K. H. Welge, J. Chem. Phys. **92**, 1608 (1990).

[24] K. C. Kulander, Chem. Phys. Lett. **103**, 373 (1984).

[25] R. N. Dixon, C. C. Marston, and G. G. Balint-Kurti, J. Chem. Phys. **93**, 6520 (1990).

[26] U. Fano, Phys. Rev. **124**, 1866 (1961).

[27] D. Imre, J. L. Kinsey, A. Sinha, and J. Krenos, J. Phys. Chem. **88**, 3956, (1984).

[28] L. Halonen and T. Carrington, Jr., J. Chem. Phys. **88**, 4171 (1987).

[29] M. S. Child and L. Halonen, Adv. Chem. Phys. **57**, 1 (1984). See also the vibrational eigenstates of H_2O depicted in Fig. 1B in L. Xiao and M. E. Kellman, J. Chem. Phys. **93**, 5805 (1990); of the six vibrational eigenstates with five quanta in OH stretching, four are local mode in character and two are best described in a normal mode representation.

[30] For information on sum frequency generation in BBO, see W. L. Glab and J. P. Hessler, Appl. Opt. **26**, 3181 (1987).

[31] GAUSSIAN 92 Revision C, M. J. Frisch, G. W. Trucks, M. Head-Gordon, P. M. W. Gill, M. W. Wong, J. B. Foresman, B. G. Johnson, H. B. Schlegel, M. A. Robb, E. S. Replogle, R. Gomperts, J. L. Andres, K. Raghavachari, J. S. Binkley, C. Gonzalez, R. L. Martin, D. J. Fox, D. J. Defrees, J. Baker, J. J. P. Stewart, and J. A. Pople, (Gaussian, Inc., Pittsburgh, PA, 1992).

[32] Less than 1% of room temperature H_2S is in vibrationally excited states.

[33] Schinke and co-workers describe the dissociative surface as a diabat of $^1A_2$ symmetry, but this surface is actually from an adiabatic linear combination of two antibonding electronic states localized on either S–H bond. (See Fig. 5, lower orbitals, for a picture of the S–H antibonding orbitals involved.)

[34] R. J. Sension, R. L. Brudzynski, and B. S. Hudson, Phys. Rev. Lett. **61**, 694 (1988).

[35] The emitted photon energy is roughly determined by the difference in potential energy between the point on the excited state surface at the conical intersection and the energy of the ground state potential at the same geometry so the emission reflecting the dynamics appears in higher eigenstates the higher the absorbed photon energy ($h\nu_{abs}-h\nu_{emit}$=final vibrational state energy).